Biogeosciences Discuss., 11, 7485–7519, 2014
www.biogeosciences-discuss.net/11/7485/2014/
doi:10.5194/bgd-11-7485-2014

Biogeosciences Discussions
Open Access

Inorganic carbon dynamics of melt pond-covered first year sea ice in the Canadian Arctic

N.-X. Geilfus[1,2], R. J. Galley[1], O. Crabeck[1], T. Papakyriakou[1], J. Landy[1], J.-L. Tison[3], and S. Rysgaard[1,2,4]

[1]Centre for Earth Observation Science, Department of Environment and Geography, University of Manitoba, Winnipeg, Canada
[2]Arctic Research Centre, Aarhus University, Aarhus, Denmark
[3]Laboratoire de Glaciologie, DSTE, Université Libre de Bruxelles, Brussels, Belgium
[4]Greenland Climate Research Centre, Greenland Institute of Natural Resources, Nuuk, Greenland

Received: 26 March 2014 – Accepted: 12 May 2014 – Published: 23 May 2014

Correspondence to: N.-X. Geilfus (geilfus@biology.au.dk)

Published by Copernicus Publications on behalf of the European Geosciences Union.

Abstract

Melt pond formation is a common feature of the spring and summer Arctic sea ice. However, the role of the melt ponds formation and the impact of the sea ice melt on both the direction and size of CO_2 flux between air and sea is still unknown. Here we describe the CO_2-carbonate chemistry of melting sea ice, melt ponds and the underlying seawater associated with measurement of CO_2 fluxes across first year landfast sea ice in the Resolute Passage, Nunavut, in June 2012.

Early in the melt season, the increase of the ice temperature and the subsequent decrease of the bulk ice salinity promote a strong decrease of the total alkalinity (TA), total dissolved inorganic carbon (TCO_2) and partial pressure of CO_2 (pCO_2) within the bulk sea ice and the brine. Later on, melt pond formation affects both the bulk sea ice and the brine system. As melt ponds are formed from melted snow the in situ melt pond pCO_2 is low (36 µatm). The percolation of this low pCO_2 melt water into the sea ice matrix dilutes the brine resulting in a strong decrease of the in situ brine pCO_2 (to 20 µatm). As melt ponds reach equilibrium with the atmosphere, their in situ pCO_2 increase (up to 380 µatm) and the percolation of this high concentration pCO_2 melt water increase the in situ brine pCO_2 within the sea ice matrix.

The low in situ pCO_2 observed in brine and melt ponds results in CO_2 fluxes of -0.04 to -5.4 mmol m^{-2} d^{-1}. As melt ponds reach equilibrium with the atmosphere, the uptake becomes less significant. However, since melt ponds are continuously supplied by melt water their in situ pCO_2 still remains low, promoting a continuous but moderate uptake of CO_2 (~ -1 mmol m^{-2} d^{-1}).

The potential uptake of atmospheric CO_2 by melting sea ice during the Arctic summer has been estimated from 7 to 16 Tg of C ignoring the role of melt ponds. This additional uptake of CO_2 associated to Arctic sea ice needs to be further explored and considered in the estimation of the Arctic Ocean's overall CO_2 budget.

BGD
11, 7485–7519, 2014

1 Introduction

The Arctic Ocean represents a globally important CO_2 sink with current estimates of net air to sea CO_2 fluxes between −66 and −199 Tg C yr^{-1} (Bates and Mathis, 2009; Takahashi et al., 2009). The role of sea ice in these measured air–sea CO_2 exchanges still remains uncertain (Parmentier et al., 2013) although recent studies suggest that sea ice may act as an important control on the CO_2 partial pressure (pCO_2) in the ocean surface layer (e.g. Rysgaard et al., 2007, 2012b, 2013b). Our understanding of inorganic carbon dynamics during the sea ice melt season and its importance to the annual exchange of CO_2 across the atmosphere–sea ice–ocean interfaces is incomplete. Melt ponds have been invoked as significant contributors to the Arctic CO_2 balance through their uptake of CO_2 (Semiletov et al., 2004). However, their impact on inorganic carbon transport through sea ice remains largely uncharacterized, despite the fact that they are a major and increasing surface feature of Arctic sea ice during spring and summer (Rösel and Kaleschke, 2012).

Melt ponds cover up to 50–60 % of the Arctic summer sea ice area (Fetterer and Untersteiner, 1998; Eicken et al., 2004). They result from the accumulation of meltwater on sea ice mainly due to melting of snow. Sea ice melt also contributes to the melt pond formation and growth in advanced stages of melt (Rösel and Kaleschke, 2012), driven by the increase of short-wave radiation absorption during the summer (Taylor and Feltham, 2004). During melt pond formation, meltwater either drains into the ocean through cracks and other openings in the sea ice or is collected on the ice surface in depressed areas. This meltwater is nearly free of salt and has a density maximum above the freezing point. Therefore, the radiative heating will favour convection (Fetterer and Untersteiner, 1998). This convection will be further assisted by winds, increasing temperature erosion of the pond edge eventually extending the pond area. As sea ice warms during spring its brine volume increases and meltwater ponds located above the freeboard may drain by vertical seepage to the underlying water (brine flushing – e.g. Fetterer and Untersteiner, 1998), thereby freshening the upper layer of the

BGD
11, 7485–7519, 2014

ocean. This mechanism is believed to be the primary cause for sea ice desalinisation (Untersteiner, 1968; Cox and Weeks, 1974). The input of freshwater to the surface layer of the ocean can lead to the formation of under-ice melt ponds, freshwater lenses trapped under thinner ice areas or in depressions in the bottom of thicker ice (Hanson, 1965; Weeks, 2010). The discharge of melt water through the ice cover is proportional to the ice permeability and the hydraulic pressure gradient in the brine system. In summer Arctic sea ice, this gradient is mostly determined by differences in hydraulic head that develop as a result of melt over a nonuniform ice surface (Eicken et al., 2002).

Melt pond formation has a strong impact on the summer energy and mass budgets of an ice cover through the sea ice–albedo-feedback mechanism (Fetterer and Untersteiner, 1998; Taylor and Feltham, 2004; Perovich et al., 2011). Melt ponds also alter the physical and optical properties of sea ice (Perovich et al., 2002), have a strong influence of the temporal evolution of sea ice salinity (Untersteiner, 1968; Cox and Weeks, 1974) and affect the salt and heat budget of the ocean mixed layer (Eicken et al., 2002; Perovich et al., 2002). Although a few studies report surface flux measurements of CO_2 during active surface melt (Semiletov et al., 2004; Geilfus et al., 2012b; Nomura et al., 2013), the role of surface melt ponds and the impact of sea ice melt on both the direction and the amount of air–sea CO_2 flux is still not well understood.

Semiletov et al. (2004), using chambers, documented CO_2 fluxes of −3.9 to $-51\,\mathrm{mmol\,m^{-2}\,d^{-1}}$ (negative flux indicating sea ice uptake of CO_2) across the sea ice–atmosphere interface over melt ponds in June, near to Barrow, Alaska. At that time brine pCO_2 was undersaturated (from 220 to 280 µatm) with respect to the atmosphere (365–375 µatm). This undersaturation was attributed to an increase of photosynthetically active radiation (PAR), which was postulated to have reduced the pCO_2 in the brine by enhancing photosynthesis (Semiletov et al., 2004). In June 2008, Geilfus et al. (2012b) reported CO_2 fluxes over melt ponds and sea ice ranging from −0.02 to $-2.7\,\mathrm{mmol\,m^{-2}\,d^{-1}}$, also using the chamber technique over first year sea ice in the Beaufort Sea. Though these fluxes were substantially smaller than those reported by Semiletov et al. (2004), they were of the same order of magnitude as those reported

BGD
11, 7485–7519, 2014

during period of melt and surface flooding on Antarctic and Arctic sea ice (Nomura et al., 2013). In the Geilfus et al. (2012b) study, sea ice brine and overlying melt ponds were highly undersaturated in CO_2 relative to atmospheric levels (pCO_2 between 0 to 188 µatm and 79 to 348 µatm for brine and melt ponds respectively) for the 1.2 m thick landfast sea ice in the Amundsen Gulf (Beaufort Sea). At that time, the melt ponds were well established and interconnected. The fresh water originating from internal and surface melting was suggested as an important driver of the observed undersaturation together with other processes, including the dissolution of calcium carbonate and the primary production. Using micrometeorological techniques, Papakyriakou and Miller (2011) also reported CO_2 uptake with the progression of melt, although flux magnitudes are widely diverging from the chamber-based studies highlighted above.

In this study, we examine how the melting of the sea ice cover and the associated formation of melt ponds affects the inorganic carbon dynamic and the air–ice CO_2 exchanges. The evolution of the carbonate system was examined using measurements of TA, TCO_2 and pCO_2 performed on bulk sea ice, brine and melt ponds, in association with CO_2 flux measurements over sea ice and melt ponds. The percolation of the melt water from melt ponds was tracked using the isotopic ratios δD and δ^{18}O within bulk sea ice and brine.

2 Study site, materials and methods

Field data were collected over first-year landfast sea ice in Resolute Passage, Nunavut, from 3 to 23 June 2012. The sampling site (~ 100 m × 100 m) was located between Sheringham Point and Griffith Island (74.726° N, 95.576° W, Fig. 1). At the site, adjacent 5 m × 5 m areas were chosen for regular sampling for carbonate chemistry determination of ice cores and seawater (on 4 day intervals), while the carbonate chemistry of brine and the surface flux of CO_2 was sampled every 2 days. During our survey, the air temperature increased from 0.6 to 3.2 °C, with a maximum temperature of 4.3 °C observed on 19 June (Fig. 2). During our first ice station (4 June), coarse wet snow

BGD
11, 7485–7519, 2014

was found at the surface of the ice. On 10 June, the first melt ponds were observed (Fig. 2). Once the melt ponds started to form, the ice core and brine sampling was limited to area without melt ponds, referred to as melt hummock.

Brine was collected using the sackhole technique (e.g. Gleitz et al., 1995). Sackholes were drilled at incrementing depths (20, 40, 75, 100 cm). Brine from adjacent brine channels and pockets was allowed to seep into the sackholes for 5 to 10 min before being collected using a peristaltic pump (Cole Palmer®, Masterflex – Environmental Sampler). Each sackhole was covered with a plastic lid to avoid the intrusion of snow and snow and ice melt.

Sea ice core samples were collected using a MARK II coring system (Kovacs Enterprises®). Two ice cores were immediately wrapped in polyethylene (PE) bags and stored horizontally on the sampling site at −20 °C in a portable freezer (Whynter® 45 Quart portable Freezer FM-45G) to minimize brine drainage during transport. The first core was dedicated to the analysis of total alkalinity (TA) and total dissolved inorganic carbon (TCO_2). The second core was dedicated to partial pressure of CO_2 in bulk ice (bulk ice pCO_2) analysis. Two others cores were collected for in situ sea ice temperature, bulk ice salinity and ikaite ($CaCO_3 \cdot 6H_2O$) content.

Seawater was collected at the ice–water interface through an ice core hole using the peristaltic pump. The same pump was used to collected melt pond samples and an articulated arm was used to collect under-ice melt pond samples. We also collected water column samples at six depths (2, 5, 10, 25, 50, 80 m) using 5 L Niskin bottles for determination of TA and TCO_2. Vertical profiles of water temperature and salinity were measured with a newly calibrated Sea-Bird SBE 19plus V2 conductivity-temperature depth (CTD) probe.

The pCO_2 was measured in situ on brine, melt pond water and under-ice seawater using a custom-made equilibration system. The system consists of a membrane contractor equilibrator connected to a non-dispersive infrared gas analyzer (IRGA, Li-Cor 820) via a closed air loop. Brine and airflow rates through the equilibrator and IRGA are approximately 2 L min^{-1} and 3 L min^{-1}, respectively. Temperature was measured

BGD
11, 7485–7519, 2014

using a calibrated temperature probe (Testo 720®, ±0.1 °C precision) simultaneously in situ and at the outlet of the equilibrator. Temperature correction of pCO_2 was applied assuming that the relation of Copin Montégut (1988) is valid at low temperature and high salinity.

Sea ice temperature was measured in situ immediately after extraction of the ice cores using a calibrated temperature probe (Testo 720®, ±0.1 °C precision) inserted into pre-drilled holes (2.5 cm intervals), perpendicular to core sides. Bulk sea ice salinity and ikaite content was determined on a duplicate ice core, sliced into 5 cm sections directly after extraction and placed in sealed containers, which were then placed in a lab fridge to melt at 4 °C. These samples were checked regularly, so that the melt water temperature never rose above 1–2 °C. Once the samples melted, crystals left in solution were observed under a binocular microscope at room temperature. Finally, the bulk salinity of these samples was measured using a calibrated Thermo-Orion portable salinometer WP-84TPS meter with a precision of ±0.1. The sea ice brine volume was calculated according to Cox and Weeks (1983) for temperatures below −2 °C, and according to Leppäranta and Manninen (1988) for temperature within the range 0 °C to −2 °C.

Samples of melted bulk ice, brine, melt pond, under-ice melt pond water and underlying seawater were bring back to the University of Manitoba for TA and TCO_2 measurements. Samples were poisoned with a solution of saturated $HgCl_2$ to prevent any biological activity. The ice core was cut into 10 cm sections in a cold room (−20 °C), and each section was placed in a gas-tight laminated (Nylon, ethylene vinyl alcohol, and polyethylene) plastic bag (Hansen et al., 2000) fitted with a 20 cm gas tight Tygon tube and valve. The plastic bag was sealed immediately and excess air was gently removed through the valve using a vacuum pump. The bagged sea ice samples were then melted in the fridge at 4 °C and the meltwater mixture and bubbles were transferred to a gas-tight vial (12 mL Exetainer, Labco High Wycombe, UK). TA was determined by potentiometric titration (Haraldsson et al., 1997) with a precision of ±3 µmol kg^{-1} while

BGD
11, 7485–7519, 2014

TCO_2 was determined by CO_2 equilibration chamber coupled to an infrared CO_2 analyzer with a precision of ±2 µmol kg^{-1}.

The ice cores taken for bulk ice pCO_2 analysis were cut into 10 cm sections and stored at −20 °C. The bulk ice pCO_2 was measured at the Laboratoire de Glaciologie, at the Université Libre de Bruxelles using the technique developed by Geilfus et al. (2012a). The general principle of the method is to equilibrate the sea ice samples with a mixture of N_2 and CO_2 of known concentration (referred to as the "standard gas", 146 µatm) at the in situ temperature and rapidly extract the gases into a Varian 3300 gas chromatograph under vacuum. The ice sample is cut to fit tightly the container (4 cm × 4 cm × 4.5 cm) to both minimize the headspace volume and keep this headspace constant. The standard gas is injected at 1013 mbar into the container. Then the container, with the ice sample, is placed in a thermostatic bath setup at the field in situ temperature for 24 h. This timing is chosen to ensure that, the sample is re-equilibrated to the brine volume and chemical conditions at the in situ temperature. During the injection to the gas chromatograph, the pressure difference between the vacuum line and the containers extracts all the CO_2 from the brine into the gas chromatograph. This method is only valid if the ice is permeable at the in situ conditions.

We determined δD and δ^{18}O in 2 mL aliquots of sea ice, brine, under-ice seawater, melt pond and under-ice melt pond. Stable isotope measurements were carried out at the University of Manitoba using a Picarro L2130-*i* analyzer. Samples were calibrated against Vienna Standard Mean Ocean Water (VSMOW) with a precision of 0.1 ‰ for ∂D and 0.025 ‰ for ∂^{18}O.

CO_2 fluxes at the sea ice surface were measured using a Licor 8100–103 chamber associated with the LI-8100A soil CO_2 flux system. The chamber was connected in a closed loop to the IRGA with an air pump rate at 3 L min^{-1}. pCO_2 in the chamber was recorded every second for 15 min and the flux was computed from the slope of the linear regression of pCO_2 against time ($r^2 > 0.99$) according to Frankignoulle (1988), taking into account the air volume enclosed within the chamber. The uncertainty of the

BGD
11, 7485–7519, 2014

flux computation due to the standard error on the regression slope was on average ±3 %.

3 Results

3.1 Sea ice

The average ice thickness at the sampling site, as determined from cores, decreased from 130 (±5) to 105 (±5) cm over the sampling campaign. The ice temperature increased from −2.9 °C on 4 June to −1.5 °C on 12 June (Fig. 3). From 10 June, the top 20 cm of the ice had a temperature slightly negative, from −0.5 °C to 0 °C while the rest of the ice thickness remained around −1.5 °C. Bulk ice salinity ranged from 7.5 to 0 (Fig. 3). The top 20 cm of the ice had salinity around 0 while the salinity of the central part of the ice decreased from 7.5 to 4 during the survey. The high temperatures allow a brine volume content in the ice higher than 5 % (data not shown).

The δ^{18}O and δD isotopic ratio ranged from 1.9 to −23.9 ‰ and 2.5 to −191.2 ‰, respectively (Fig. 3). Profiles of δ^{18}O and δD appear to follow the same trend with the lowest values observed in the top 20 cm of the ice cover. Two low events were reported in the upper 20 cm of the ice cover. The first was from 8 to 12 June with an isotopic ratio of δ^{18}O and δD as low as −23.9 and −191.2 ‰. The second was on 17 June with a δ^{18}O and δD of −15.4 and −133.7 ‰. The rest of the ice cover ranged from −2 to 1.9 ‰ for the δ^{18}O and from −7 to 2.5 ‰ for the δD.

The mean total alkalinity in melted bulk sea ice (TA_{ice}) of the entire ice column gradually decreased from 408 µmol kg^{-1} on 4 June to 283 µmol kg^{-1} on 21 June (Fig. 3). This decrease of TA_{ice} was more pronounced in the top 20 cm of the ice cover where the minimal value of 106 µmol kg^{-1} was observed on 17 June. The same trend was observed for the total inorganic carbon ($TCO_{2\,ice}$, Fig. 3). The mean $TCO_{2\,ice}$ of the entire ice column decreased from 332 µmol kg^{-1} on 4 June to 225 µmol kg^{-1} on 21 June. On 17 June, the minimum values were observed, with a mean concentration

BGD
11, 7485–7519, 2014

of 189 µmol kg^{-1}. To discard concentration – dilution effect, we normalized TA_{ice} and $TCO_{2\,ice}$ to a salinity of 5 (noted as nTA_{ice}, $nTCO_{2\,ice}$, respectively). The main change observed in the ice cover occurs in the top 20 cm. From 4 to 17 June, nTA_{ice} and $nTCO_{2\,ice}$ increased from 468 and 345 µmol kg^{-1} to 1762 and 1041 µmol kg^{-1} while the rest of the ice cover ranged from 337 to 564 µmol kg^{-1} and from 219 to 461 µmol kg^{-1}, respectively.

From TA_{ice} and $TCO_{2\,ice}$, the bulk ice pCO_2 (noted as $pCO_{2\,calc}$) has been computed using the CO_2 dissociation constants of Mehrbach et al. (1973) refitted by Dickson and Millero (1987). We assumed a conservative behaviour of dissociation constants for the range of temperature and salinity encountered in the ice cover. This $pCO_{2\,calc}$ ranged from 0 to 32 µatm (Fig. 4). On a duplicate ice core, the bulk ice pCO_2 was also measured on solid ice, at the in situ temperature, using the sample equilibration technique developed by Geilfus et al. (2012a) (noted as $pCO_{2\,insitu}$). The $pCO_{2\,insitu}$ ranged from 6 to 182 µatm (Fig. 4).

We observed few ikaite crystals in the ice, which dissolved within a few minutes at room temperature. Due to technical problems we were unable to take any pictures of the crystals. However, as the overall aspect of these crystals look exactly as the crystals found in Geilfus et al. (2013a, b) and Rysgaard et al. (2013a, b) and as they dissolved quickly at room temperature, we assumed they were ikaite (after Rysgaard et al., 2012b, 2013a, b).

3.2 Brine

From 4 to 10 June , the brine salinity decreased from 55 to 23 (Fig. 5). Starting on 10 June, low brine salinities (ranging from 1.6 to 11.8) were found at 20 cm depth while deeper brine ranged from 11 to 30, except on 17 June where low salinity were also found at the 40 cm depth. The $\delta^{18}O$ and δD isotopic ratios ranged from −1.5 to −15.2 ‰ and from −15.5 to −118.2 ‰, respectively (Fig. 5). Both profiles appear to be similar, with the lowest values observed at 20 cm depth on 10 June (−15.2 ‰ and

BGD
11, 7485–7519, 2014

−118.1 ‰, respectively) and at 20 and 40 cm depth on 17 June (−10.4 ‰ and −87.5 ‰, respectively).

From 4 to 21 June , TA_{br} and TCO_{2br} decreased from their maximum values of 3487 and 3189 µmol kg^{-1}, to 234 and 270 µmol kg^{-1}, respectively (Fig. 5). Two periods of low concentrations were observed during our survey. First, on 10 June, minimums of TA_{br} and TCO_{2br} of 501 and 401 µmol kg^{-1} respectively, occurred at 20 cm. Then, on 17 June, TA_{br} and TCO_{2br} were at 240 and 275 µmol kg^{-1} respectively, at 20 and 40 cm. These two minimums in TA_{br} and TCO_{2br} coincided with maximums in TA_{br} and TCO_{2br} normalized to a salinity of 5 (noted as nTA_{br} and $nTCO_{2br}$). On 10 June, nTA_{br} and $nTCO_{2br}$ were at 596 and 478 µmol kg^{-1}, and on 17 June, nTA_{br} and $nTCO_{2br}$ were at 874 and 900 µmol kg^{-1}.

The in situ brine pCO_2 was under-saturated with respect to the atmosphere (395 µatm in June 2012) with concentrations ranging from 20 µatm to 389 µatm (Figs. 4 and 5). From 4 to 12 June, the mean in situ brine pCO_2 decreased from 344 to 70 µatm. Then, it increased to 246 µatm on 17 June before decreasing to 81 µatm on 21 June.

3.3 Melt ponds

On 10 June, melt ponds started to form at the surface of the ice cover and were present during the rest of the survey. The melt pond salinity ranged from 1.5 to 2.4 with temperatures from 0 °C to 0.4 °C. The $\delta^{18}O$ and δD isotopic ratios ranged from −3.8 to −10.1 ‰ and from −40.6 to −93.4 ‰.

TA_{mp} ranged from 219 to 332 µmol kg^{-1} and TCO_{2mp} ranged from 206 to 306 µmol kg^{-1} over the study period. Normalized TA and TCO_2 in the melt ponds (nTA_{mp} and $nTCO_{2mp}$) ranged from 489 to 972 µmol kg^{-1} and 562 to 918 µmol kg^{-1}, respectively.

Melt pond water was also under-saturated with respect to the atmosphere with a pCO_2 concentrations ranging from 36 to 381 µatm. During the initial formation of

BGD
11, 7485–7519, 2014

melt ponds, their pCO_2 was low (36–84 µatm) but increased to 381 µatm on 17 June before fluctuating between 150 and 370 µatm.

3.4 Underlying seawater

During the survey, the temperature of the seawater layer immediately underlying the sea ice increased from −1.7 °C to −1.4 °C. The salinity of this layer decreased gradually from 33.2 to 31.4 while the salinity of the water column below 10 m changed much less (Fig. 6).

The $\delta^{18}O$ and δD isotopic ratio of the surface layer decreased gradually from their respective minimums of −1.3 and −17.3 ‰ to −2.2 and −19.5 ‰ on 20 June. Deeper layers of the water column ranged from −1.5 and −14.9 ‰ to −1.9 and −18.9 ‰, respectively (Fig. 6).

TA_{sw} and $TCO_{2\,sw}$ ranged from 2021 and 1920 µmol kg^{-1} to 2239 and 2167 µmol kg^{-1}, respectively. On 20 June, a strong decrease in TA_{sw} and $TCO_{2\,sw}$ was observed, leading to the observed minimum values at the surface of the water column. The normalized TA_{sw} and $TCO_{2\,sw}$ (nTA_{sw} and $nTCO_{2\,sw}$ to salinity 5 are shown (Fig. 6) to allow direct comparison with the sea ice and brine data) ranged from 319 to 350 µmol kg^{-1} and 303 to 333 µmol kg^{-1}, respectively.

The in situ pCO_2 at the seawater surface ranged from 259 to 469 µatm, shifting from an oversaturated state (455 µatm) on 7 June to an under saturated one (259 µatm) after 21 and 23 June (Fig. 6).

3.5 Air–ice CO_2 fluxes

CO_2 fluxes were systematically measured over sea ice and melt ponds (Fig. 7) throughout the campaign. Initially, CO_2 fluxes over sea ice were on average at −1.38 mmol m^{-2} d^{-1} (negative flux denoting uptake of CO_2). During the initial formation of melt ponds, the fluxes over sea ice peaked at −5.4 mmol m^{-2} d^{-1} on 10 June and −2 mmol m^{-2} d^{-1} on 12 June. Over melt ponds, the initial uptake of CO_2 was signif-

BGD
11, 7485–7519, 2014

icant at $-2.9\,\mathrm{mmol\,m^{-2}\,d^{-1}}$ on 10 June and $-4.8\,\mathrm{mmol\,m^{-2}\,d^{-1}}$ on 12 June. Thereafter the uptake of CO_2 by sea ice and melt ponds decreased over time and stabilized at around $-1\,\mathrm{mmol\,m^{-2}\,d^{-1}}$.

4 Discussion

Over the course of our study period, the temperature gradient within sea ice decreased, leading to a nearly isothermal ice cover. Seasonally rising sea ice temperature was associated with decreasing bulk ice salinity, until ultimately values approached 0 at the surface of the ice cover (Fig. 3). The percolation of snowmelt through the ice cover, and its refreezing into the ice matrix, formed interposed ice. The formation of interposed ice has been described by Freitag and Eicken (2003) and Polashenski et al. (2012) and could explain the low salinity and low $\delta^{18}O$ and δD isotopic ratio found in the upper 20 cm of the ice cover.

Melt pond formation and subsequent percolation of melt water into the ice cover are visible in the brine system from the isotopic ratio data (Figs. 3 and 5). The 20 cm depth on 9 and 10 June as well as the 20 and 40 cm depth brine on 17 June had the same isotopic ratios as the melt ponds. The increase of the $\delta^{18}O$ and δD ratio in the melt ponds observed on 19 and 21 June suggests that the contribution of the sea ice melt to the melt ponds had increased. The combination of low $\delta^{18}O$ and δD values, low bulk salinities (< 5), and warm ice temperature ($\sim 0\,^{\circ}C$) collectively suggest that melt water percolated into the ice cover, at least to a depth of 40 cm (Fig. 5).

Previous work has shown brine pCO_2 to change dramatically over the period between sea ice formation and melting (Papadimitriou et al., 2004; Nomura et al., 2010a; Geilfus et al., 2012b). Increasing ice temperature is associated with a drop in brine concentration and typically brine pCO_2. Brine dilution will also promote the dissolution of ikaite that precipitated in the sea ice, augmenting a lowering in pCO_2 following the

BGD
11, 7485–7519, 2014

reaction:

$$CaCO_3 \cdot 6H_2O + CO_2 \rightleftharpoons Ca^{2+} + 2HCO_3^- + 5H_2O \quad \text{(R1)}$$

There are several reports of ikaite precipitation in Arctic sea ice (Dieckmann et al., 2010; Rysgaard et al., 2012a, 2013b; Geilfus et al., 2013a, b; Søgaard et al., 2013). In this study however only a few crystals were observed in the ice sampled, and they dissolved within minutes after melting the sea ice. Because the overall morphology of these crystals was the same as crystals identified as ikaite by x-ray diffraction during the other campaigns, we assumed they were ikaite (after Geilfus et al., 2013a, b; Rysgaard et al., 2013a, b). It is not surprising that only small amounts of ikaite crystals were observed in the ice samples as the combination of elevated temperature and brine dilution associated with melting would support the dissolution of ikaite. Indeed, Rysgaard et al. (2013a) linked the amount of ikaite content in the ice to the ice temperature, suggesting as the ice warms up/cools down, ikaite crystals will dissolve/precipitate. As previously suggested, the dissolution of ikaite crystals during sea ice melt likely contributed to a lowering of in situ brine pCO_2 according to Reaction (R1).

The concentration of TA and TCO_2 reported in melted bulk sea ice, brine and melt ponds in this study are in the same range as those reported from previous studies in the Canadian Archipelago (Rysgaard et al., 2007; Miller et al., 2011; Geilfus et al., 2012b, 2013a). The temperature increase and the subsequent salinity decrease promote the overall decrease of TA_{ice} and $TCO_{2\,ice}$ concentrations (Fig. 3). The relatively constant nTA_{ice} and $nTCO_{2\,ice}$ reported within the ice cover during the survey suggests that the dilution effect was dominant. However, the reduction in TA_{ice} and $TCO_{2\,ice}$, in the top 20 cm of the ice cover, was more pronounced after onset of melt pond formation and the formation of interposed ice. These low concentrations are associated with a significant increase of nTA_{ice} and $nTCO_{2\,ice}$ during the survey.

The reduction of the brine salinity in response to seasonal warming promoted a decrease of TA_{br} and $TCO_{2\,br}$ (Geilfus et al., 2012b). Indeed, the mean TA_{br} and $TCO_{2\,br}$ decreased from 3344 and 3037 µmol kg^{-1} on 4 June to 1221 and 1092 µmol kg^{-1} on 10 June, and further to 657 and 579 µmol kg^{-1} on 19 June, with minimums observed

BGD
11, 7485–7519, 2014

(i) at 20 cm depth on 10 June, and (ii) at 20 and 40 cm depth on 17 June (Fig. 5). Minimums in TA_{br} and TCO_{2br} were associated with minimum isotopic ratio of $\delta^{18}O$ and δD, hence we attribute the lowering in carbonate species largely to the percolation of fresh melt water from surface melt ponds. nTA_{br} and $nTCO_{2br}$ remained relatively constant, until at least a period of melt water percolation, which corresponded to a significant rise in both nTA_{br} and $nTCO_{2br}$. This increase suggests that despite the low salinity promoting the low TA and TCO_2, melt ponds and surface brine absorb CO_2 from the atmosphere.

The melt pond formation at the sea ice surface, and the subsequent percolation of melt water through the ice cover is shown to affect TA_{br} and TCO_{2br} and appears also affect the in situ brine pCO_2 (Fig. 5). From 4 to 10 June , the decrease of the in situ brine pCO_2 is mainly due to the drop in brine salinity associated with rising temperature and the dissolution of ikaite. As melt ponds begin to form, their initial pCO_2 is much lower (36–84 µatm) than the atmosphere (395 µatm). The percolation of low pCO_2 melt pond water through the ice matrix imparted a strong decrease in the in situ brine pCO_2 observed at 20 cm depth on 9 and 10 June. However, over time, the in situ melt pond pCO_2 increased through equilibration with the atmosphere (Fig. 5). The subsequent percolation of this higher pCO_2 melt water through the ice matrix corresponded with an increase in brine pCO_2 within the sea ice as was observed on 17 June. The in situ melt pond pCO_2 decreased slightly (150 µatm on 19 June) as did the brine pCO_2 (< 100 µatm) as a result of more melt water being added to the pond. On 21 June, the pCO_2 in the melt pond increased as a result of CO_2 uptake from the atmosphere.

The bulk sea ice pCO_2 measured on solid ice samples ($pCO_{2insitu}$, Fig. 4) are in the same range as those reported by Geilfus et al. (2012a) on landfast sea ice sampled during the same season in Barrow, Alaska. Ice cover characteristic was similar to our survey: nearly isotherm ice cover (approaching 0 °C), low salinity in the surface layer (0–20 cm) and melt ponds at the surface of the ice (Zhou et al., 2013). Crabeck et al. (2014) also reported $pCO_{2insitu}$ on bulk sea ice from SW Greenland. However, the

BGD
11, 7485–7519, 2014

concentrations reported in our study are in the lower end compared with the concentrations of 77–330 µatm reported by Crabeck et al. (2014). The lower concentrations during our study may be due to warmer sea ice leading to a lower pCO_2 due to brine dilution by fresh melt water. These concentrations can be compared with the pCO_2 calculated from TA_{ice} and $TCO_{2\,ice}$ ($pCO_{2\,calc}$, Fig. 4). The range of concentration of $pCO_{2\,calc}$ is in the lower end of the concentration of $pCO_{2\,insitu}$. However, indirect pCO_2 values derived from TA and TCO_2 rely on the validity of the four equilibrium constants of the aqueous carbonate system. These thermodynamic constants are assumed to be valid at subzero temperatures, but need to be tested for validity below 0 °C. Evidently, however, both calculated and measured pCO_2 reflect similar processes, that being an over-all drop in pCO_2 associated with brine dilution and the dissolution of the calcium carbonate. While the ice $pCO_{2\,calc}$ only shows a slight decrease over time, the ice $pCO_{2\,insitu}$ reveals that larger changes may occur, especially in the upper 20 cm of the ice cover (Fig. 4). The two data sets (bulk ice $pCO_{2\,insitu}$ and the in situ brine pCO_2) differ in that a significant decrease of the in situ brine pCO_2 was observed on 12 June, just after the melt ponds formation, whereas only a slight decrease was observed in the bulk ice pCO_2 time series. The percolation of melt water with low in situ pCO_2 initiated a drop of the in situ brine pCO_2 to similar concentrations as in the melt ponds. In appears the brine pCO_2 in the sea ice is dynamic beyond the pCO_2 as estimated from the bulk sea ice, rapidly responding to the infiltration of melt water of differing pCO_2. Other examples are observed on 17 June, then again on 19 and 21 June. On 17 June, the percolation through the ice matrix of melt water with higher in situ pCO_2 was associated with an increase in in situ brine pCO_2 whereas the bulk ice $pCO_{2\,insitu}$ remained constant. On 19 and 21 June, the bulk ice $pCO_{2\,insitu}$ slightly increased while the in situ melt ponds pCO_2 slightly decreased to reach the same range of concentration.

To test the sackhole technique's ability to sample uncontaminated brine, we compared TA_{br} and $TCO_{2\,br}$ with a TA and TCO_2 estimated from the calculated brine volume (Cox and Weeks, 1983; Leppäranta and Manninen, 1988) and TA_{ice} and $TCO_{2\,ice}$ (Fig. 8). Both methods yield similar TA and TCO_2 concentrations (from 102

BGD
11, 7485–7519, 2014

to 4425 µmol kg^{-1}), with a similar relationship between TA and TCO_2 with a R^2 of 0.96. The scatter between the two methods could be due to the impossibility of determining the exact original depth from which the brine seeped, especially if melt ponds are present at the surface of the ice cover.

As melt ponds developed, freshwater percolated through the ice matrix and could form a freshwater layer at the underside of the sea ice (Hanson, 1965). An accumulation of under-ice melt water was not observed during our survey. Perhaps this is because the stage of ice melt was not sufficiently advanced and/or under-ice currents effectively mixed the freshwater layer beneath the ice. The only noticeable impact of sea ice melt on the underlying seawater was observed on 20 June where the decrease of TA_{sw} and $TCO_{2\,sw}$ was associated with the low isotopic ratio of $\delta^{18}O$ and δD occurring over a very short period (Fig. 6).

As in previous studies, the relationships between nTA and $nTCO_2$ in seawater, brine and sea ice samples can be use to determine the main processes affecting the carbonate system. In Fig. 9, the dotted lines represent the response of inorganic carbon and alkalinity to different processes (after Zeebe and Wolf-Gladrow, 2001). An exchange of $CO_{2\,(gas)}$ will affect TCO_2 while TA will remain constant. The precipitation – dissolution of ikaite will affect TA and TCO_2 in a ratio of 2 : 1. Biological activity will increase TA slightly and reduce TCO_2 slightly in the ratio $TA : TCO_2 = -0.16$ (Lazar and Loya, 1991). To calculate these theoretical effects we assumed that seawater sampled at 50 m was not influenced by the overlying melting sea ice. nTA and $nTCO_2$ pairs from sea ice samples are located along the ikaite dissolution line while brine and melt pond samples are located between the ikaite dissolution line and the CO_2 uptake line, suggesting both processes occurred in combination. We posit that ikaite crystals formed in the wintertime sea ice were dissolved, thereby lowering pCO_2 and enhancing CO_2 uptake. This support the small amount of ikaite crystals observed in the sea ice. The concentration of algal biomass (Chl *a*) has been measured at the bottom of the ice and decreased from 11.1 µg L^{-1} in 4 June to 0.05 µg L^{-1} on 21 June (unpublished data, C. Mundy). These concentrations are in the same range as those reported by Mundy

BGD
11, 7485–7519, 2014

et al. (2011) and Geilfus et al. (2012b) on melting landfast sea ice in the Beaufort Sea. As the Chl *a* concentration decreased while the in situ brine pCO_2 oscillated greatly during this survey (Fig. 5), this suggests that biological processes are only marginally affecting the carbonate system. Geilfus et al. (2012b) and Papadimitriou et al. (2012) observed a similar trend in the Beaufort Sea (Arctic) and in the Weddell Sea (Antarctica) on landfast sea ice during an early spring, but at ice temperatures colder than observed during the present study. Therefore sea ice and brine samples from these studies fell on the other side of the seawater value, lying between the precipitation of calcium carbonate and the release of CO_2, in the TA/TCO_2 space.

The CO_2 fluxes reported during this study are lower than fluxes reported by Semiletov et al. (2004) over melt ponds, but similar to fluxes reported by Geilfus et al. (2012b) over sea ice and melt ponds and similar to fluxes reported by Nomura et al. (2013) on Antarctic and Arctic sea ice during periods of snowmelt and surface flooding. CO_2 fluxes over sea ice depend on the ice permeability and the CO_2 concentration gradient between the ice surface and the atmosphere conveyed through the liquid phase (i.e. brine and melt water). Brine and melt ponds were under-saturated with respect to the atmosphere (Fig. 5). The sea ice uptake of atmospheric CO_2 was at first moderate ($\sim -1\,\mathrm{mmol\,m^{-2}\,d^{-1}}$, Fig. 7) due to brine being slightly undersaturated. Then the decrease of the in situ brine pCO_2 due to the percolation of melt ponds with low in situ pCO_2 intensified the uptake of atmospheric CO_2 (up to $-5.4\,\mathrm{mmol\,m^{-2}\,d^{-1}}$) by the ice. As the in situ brine pCO_2 increased, the uptake of CO_2 decreased accordingly ($\sim -1\,\mathrm{mmol\,m^{-2}\,d^{-1}}$). In addition, insignificant fluxes (in the range of $-0.005\,\mathrm{mmol\,m^{-2}\,d^{-1}}$) were detected over superimposed ice, as reported by Nomura et al. (2010b) and Geilfus et al. (2012b). During the initial formation of melt ponds, the low in situ pCO_2 promoted a strong uptake of atmospheric CO_2 ($-3.8\,\mathrm{mmol\,m^{-2}\,d^{-1}}$). However, as the melt pond pCO_2 approached equilibrium with the atmosphere, their CO_2 uptake decreased and stabilized around $\sim -1\,\mathrm{mmol\,m^{-2}\,d^{-1}}$.

To estimate a total uptake of atmospheric CO_2 (Fig. 7) over the sampling area (F_{tot}), we used the pond coverage (x) (Fig. 2) to weight the fluxes over sea ice (F_{ice}) and over

BGD
11, 7485–7519, 2014

melt ponds (F_{mp}), respectively, using the following equation:

$$F_{tot} = F_{ice} \cdot (1 - x) + F_{mp} \cdot x$$

The pond coverage (Fig. 2) was obtained six times between the date of pond onset (10 June) and the final sampling date, with a terrestrial laser scanner. In short, the scanner was used to measure the surface topography of an untouched 80 × 160 m area of sea ice and could also differentiate between ice cover and melt ponds at the surface, thereby providing the pond fraction (Landy et al., 2014). F_{tot} peaked during the initial formation of the melt ponds, then return to previous values ($-1\,\mathrm{mmol\,m^{-2}\,d^{-1}}$) when melt ponds are dominating. pCO_2 conditions in melt ponds are determined by a balance between equilibration with atmospheric CO_2 the continuous supply of melt water from the snow and sea ice. This allows melt ponds to be a continuous but moderate CO_2 sink. Therefore, if we take into account a mean uptake of CO_2 of $-1\,\mathrm{mmol\,m^{-2}\,d^{-1}}$, over the total area of the Arctic sea ice during spring and summer thaw (90 days), we derive an uptake of 16.4 Tg of carbon. Rysgaard et al. (2011) estimated an overall budget for the Arctic sea ice between 14 and 31 Tg of C depending on whether the precipitation of calcium carbonate took place in the ice or not. Other estimates of carbon uptake by the Arctic Ocean include Takahashi et al. (2009), who estimated an uptake of 121 Tg of C $\mathrm{yr^{-1}}$ for an area north of 66° N while Bates and Mathis (2009) estimated an uptake between 66 and 199 Tg of C $\mathrm{yr^{-1}}$ for the Arctic Ocean. However, these works ignored the role of the Arctic sea ice and considered it as an impermeable barrier, impeding the gas exchanges between the ocean and the atmosphere. As we have shown in the present study, things may be more complicated and in fact sea ice may play an important role in mediating the exchange of CO_2 between the atmosphere and ocean at high-latitude areas.

BGD
11, 7485–7519, 2014

5 Conclusions

We investigated the evolution of the inorganic carbon within landfast first-year sea ice in Resolute Passage, Nunavut, from 3 to 23 June 2012. During our survey, the ice was melting due to the high atmospheric temperature and absorption of solar radiation. Temperature profiles became isothermal ($\sim -1\,^{\circ}$C) with low salinity at the surface (~ 0) and melt ponds started to form at the surface of the ice on 10 June.

Early in the melt period, increased ice temperatures and subsequent decreased bulk ice salinity dissolution of ikaite crystals promoted a strong decrease of TA, TCO_2 and pCO_2 observed in bulk sea ice and brines (Fig. 10). The decrease of pCO_2 causes sea ice to act as a sink for the atmospheric CO_2 ($\sim -1\,\mathrm{mmol\,m^{-2}\,d^{-1}}$). This sink increases (up to $-5.4\,\mathrm{mmol\,m^{-2}\,d^{-1}}$) during the initial formation of melt pond due to its very low pCO_2 levels. The percolation of melt pond water into the ice matrix will intensify the brine dilution and the decrease of the brine TA, TCO_2 and pCO_2 (Fig. 10). The low TA_{br} and TCO_{2br} concentrations observed were associated with the percolation of melt water from melt ponds, and the in situ brine pCO_2 seemed also to be controlled by the melt ponds. As melt ponds forms from melted snow and melted ice surface the in situ melt pond pCO_2 is low (36 µatm). The percolation of this low pCO_2 melt water into the sea ice matrix dilutes the brine causing the in situ brine pCO_2 to decrease (20 µatm). As temperature rises, melt water is continuously supplied to the ponds, which prevents melt pond from fully equilibrating with the atmospheric CO_2. Instead, pCO_2 in the melt ponds fluctuates between 0 µatm and the atmospheric concentration (395 µatm). As melt ponds reach equilibrium with the atmosphere, the uptake becomes less significant. But as melt ponds are continuously supplied with fresh melt water while simultaneously draining to the ocean, their in situ pCO_2 remains undersaturated and hereby promote a continuous but moderate uptake of CO_2 from the atmosphere ($\sim -1\,\mathrm{mmol\,m^{-2}\,d^{-1}}$).

Based on the present study, we estimate the CO_2 flux due to melt ponds in the Arctic to be in the order of -7 to -16 Tg of C. This is 5–15 % of the total uptake for the Arctic Ocean previously reported (Bates and Mathis, 2009; Takahashi et al., 2009).

BGD
11, 7485–7519, 2014

Acknowledgements. This study was funded by the Canada Excellence Research Chair (CERC, S. R.), the Natural Sciences and Engineering Research Council (NSERC) of Canada (T. P.) and from the Bigsouth Belspo project (J.-L. T.) # SD/CA/05A. This work is a contribution to the Arctic Science Partnership (ASP), the ArcticNet Networks of Centres of Excellence programs and the SCOR BEPSII project.

References

Bates, N. R. and Mathis, J. T.: The Arctic Ocean marine carbon cycle: evaluation of air–sea CO_2 exchanges, ocean acidification impacts and potential feedbacks, Biogeosciences, 6, 2433–2459, doi:10.5194/bg-6-2433-2009, 2009.

Copin Montégut, C.: A new formula for the effect of temperature on the partial pressure of carbon dioxide in seawater, Mar. Chem., 25, 29–37, 1988.

Cox, G. F. N. and Weeks, W. F.: Salinity variations in sea ice, J. Glaciol., 13, 109–120, 1974.

Cox, G. F. N. and Weeks, W. F.: Equations for determining the gas and brine volumes in sea-ice samples, J. Glaciol., 29, 306–316, 1983.

Crabeck, O., Delille, B., Thomas, D. N., Geilfus, N. X., Rysgaard, S., and Tison, J. L.: CO_2 and CH_4 in sea ice from a subarctic fjord, Biogeosciences Discuss., 11, 4047–4083, doi:10.5194/bgd-11-4047-2014, 2014.

Dickson, A. G. and Millero, F. J.: A comparison of the equilibrium constants for the dissociation of carbonic acid in seawater media, Deep-Sea Res. Pt. I, 34, 1733–1743, 1987.

Dieckmann, G. S., Nehrke, G., Uhlig, C., Göttlicher, J., Gerland, S., Granskog, M. A., and Thomas, D. N.: Brief Communication: Ikaite ($CaCO_3 \cdot 6H_2O$) discovered in Arctic sea ice, The Cryosphere, 4, 227–230, doi:10.5194/tc-4-227-2010, 2010.

Eicken, H., Krouse, H. R., Kadko, D., and Perovich, D. K.: Tracer studies of pathways and rates of meltwater transport through Arctic summer sea ice, J. Geophys. Res.-Oceans, 107, 8046, doi:10.1029/2000JC000583, 2002.

Eicken, H., Grenfell, T. C., Perovich, D. K., Richter-Menge, J. A., and Frey, K.: Hydraulic controls of summer Arctic pack ice albedo, J. Geophys. Res.-Oceans, 109, C08007, doi:10.1029/2003JC001989, 2004.

Fetterer, F. and Untersteiner, N.: Observations of melt ponds on Arctic sea ice, J. Geophys. Res.-Oceans, 103, 24821–24835, 1998.

BGD
11, 7485–7519, 2014

Frankignoulle, M.: Field-measurements of air sea CO_2 exchange, Limnol. Oceanogr., 33, 313–322, 1988.
Freitag, J. and Eicken, H.: Meltwater circulation and permeability of Arctic summer sea ice derived from hydrological field experiments, J. Glaciol., 49, 349–358, 2003.
Geilfus, N. X., Delille, B., Verbeke, V., and Tison, J. L.: Towards a method for high vertical resolution measurements of the partial pressure of CO_2 within bulk sea ice, J. Glaciol., 58, 287–300, 2012a.
Geilfus, N. X., Carnat, G., Papakyriakou, T., Tison, J. L., Else, B., Thomas, H., Shadwick, E., and Delille, B.: Dynamics of pCO_2 and related air–ice CO_2 fluxes in the Arctic coastal zone (Amundsen Gulf, Beaufort Sea), J. Geophys. Res.-Oceans, 117, C00G10, doi:10.1029/2011JC007118, 2012b.
Geilfus, N. X., Carnat, G., Dieckmann, G. S., Halden, N., Nehrke, G., Papakyriakou, T., Tison, J. L., and Delille, B.: First estimates of the contribution of $CaCO_3$ precipitation to the release of CO_2 to the atmosphere during young sea ice growth, J. Geophys. Res., 118, 244–255, doi:10.1029/2012JC007980, 2013a.
Geilfus, N. X., Galley, R. J., Cooper, M., Halden, N., Hare, A., Wang, F., Søgaard, D. H., and Rysgaard, S.: Gypsum crystals observed in experimental and natural sea ice, Geophys. Res. Lett., 40, 6362–6367, doi:10.1002/2013GL058479, 2013b.
Gleitz, M., v. d. Loeff, M. R., Thomas, D. N., Dieckmann, G. S., and Millero, F. J.: Comparison of summer and winter inorganic carbon, oxygen and nutrient concentrations in Antarctic sea ice brine, Mar. Chem., 51, 81–91, 1995.
Hansen, J. W., Thamdrup, B., and Jørgensen, B. B.: Anoxic incubation of sediment in gas-tight plastic bags: a method for biogeochemical processes studies, Mar. Ecol.-Prog. Ser., 208, 273–282, 2000.
Hanson, A. M.: Studies of the mass budget of arctic pack-ice floes, J. Glaciol., 5, 701–709, 1965.
Haraldsson, C., Anderson, L. G., Hassellov, M., Hulth, S., and Olsson, K.: Rapid, high-precision potentiometric titration of alkalinity in ocean and sediment pore waters, Deep-Sea Res. Pt. I, 44, 2031–2044, 1997.
Landy, J. C., Ehn, J. K., Shields, M., and Barber, D. G.: Surface melt pond evolution on landfast first-year sea ice in the Canadian Arctic Archipelago, J. Geophys. Res., accepted, doi:10.1002/2013JC009617, 2014.

BGD
11, 7485–7519, 2014

Lazar, B. and Loya, Y.: Bioerosion of coral reefs – a chemical approach, Limnol. Oceanogr., 36, 377–383, 1991.
Leppäranta, M. and Manninen, T.: The brine and gas content of sea ice with attention to low salinities and high temperatures, Rep., Helsinki, 1988.
Mehrbach, C., Culberson, C. H., Hawley, J. E., and Pytkowicz, R. M.: Measurements of the apparent dissociation constants of carbonic acid in seawater at atmospheric pressure, Limnol. Oceanogr., 18, 897–907, 1973.
Miller, L. A., Carnat, G., Else, B. G. T., Sutherland, N., and Papakyriakou, T. N.: Carbonate system evolution at the Arctic Ocean surface during autumn freeze-up, J. Geophys. Res., 111, C00G04, doi:10.1029/2011JC007143, 2011.
Mundy, C. J., Gosselin, M., Ehn, J. K., Belzile, C., Poulin, M., Alou, E., Roy, S., Hop, H., Lessard, S., Papakyriakou, T. N., Barber, D. G., and Stewart, J.: Characteristics of two distinct high-light acclimated algal communities during advanced stages of sea ice melt, Polar Biol., 34, 1869–1886, 2011.
Nomura, D., Eicken, H., Gradinger, R., and Shirasawa, K.: Rapid physically driven inversion of the air–sea ice CO_2 flux in the seasonal landfast ice off Barrow, Alaska after onset surface melt, Cont. Shelf. Res., 30, 1998–2004, 2010a.
Nomura, D., Yoshikawa-Inoue, H., Toyota, T., and Shirasawa, K.: Effects of snow, snow-melting and re-freezing processes on air–sea ice CO_2 flux, J. Glaciol., 56, 262–270, 2010b.
Nomura, D., Granskog, M. A., Assmy, P., Simizu, D., and Hashida, G.: Arctic and Antarctic sea ice acts as a sink for atmospheric CO_2 during periods of snowmelt and surface flooding, J. Geophys. Res.-Oceans, 118, 6511–6524, doi:10.1002/2013JC009048, 2013.
Papadimitriou, S., Kennedy, H., Kattner, G., Dieckmann, G. S., and Thomas, D. N.: Experimental evidence for carbonate precipitation and CO_2 degassing during sea ice formation, Geochim. Cosmochim. Ac., 68, 1749–1761, 2004.
Papadimitriou, S., Kennedy, H., Norman, L., Kennedy, D. P., Dieckmann, G. S., and Thomas, D. N.: The effect of biological activity, $CaCO_3$ mineral dynamics, and CO_2 degassing in the inorganic carbon cycle in sea ice and late winter-early spring in the Weddell Sea, Antarctica, J. Geophys. Res., 117, C08011, doi:10.1029/2012JC008058, 2012.
Papakyriakou, T. and Miller, L.: Springtime CO_2 exchange over seasonal sea ice in the Canadian Arctic Archipelago, Ann. Glaciol., 52, 215–224, doi:10.3189/172756411795931534, 2011.

BGD
11, 7485–7519, 2014

Parmentier, F.-J. W., Christensen, T. R., Sørensen, L. L., Rysgaard, S., McGuire, A. D., Miller, P. A., and Walker, D. A.: The impact of lower sea-ice extent on Arctic greenhouse-gas exchange, Nat. Clim. Change, 3, 195–202, doi:10.1038/NCLIMATE1784, 2013.

Perovich, D. K., Tucker, W. B., and Ligett, K. A.: Aerial observations of the evolution of ice surface conditions during summer, J. Geophys. Res.-Oceans, 107, 8048, doi:10.1029/2000JC000449, 2002.

Perovich, D. K., Jones, K. F., Light, B., Eicken, H., Markus, T., Stroeve, J., and Lindsay, R.: Solar partitioning in a changing Arctic sea-ice cover, Ann. Glaciol., 52, 192–196, 2011.

Polashenski, C., Perovich, D., and Courville, Z.: The mechanisms of sea ice melt pond formation and evolution, J. Geophys. Res.-Oceans, 117, C01001, doi:10.1029/2011JC007231, 2012.

Rösel, A. and Kaleschke, L.: Exceptional melt pond occurrence in the years 2007 and 2011 on the Arctic sea ice revealed from MODIS satellite data, J. Geophys. Res.-Oceans, 117, C05018, doi:10.1029/2011JC007869, 2012.

Rysgaard, S., Glud, R. N., Sejr, M. K., Bendtsen, J., and Christensen, P. B.: Inorganic carbon transport during sea ice growth and decay: a carbon pump in polar seas, J. Geophys. Res.-Oceans, 112, C03016, doi:10.1029/2006JC003572, 2007.

Rysgaard, S., Bendtsen, J., Delille, B., Dieckmann, G. S., Glud, R. N., Kennedy, H., Mortensen, J., Papadimitriou, S., Thomas, D. N., and Tison, J. L.: Sea ice contribution to the air–sea CO_2 exchange in the Arctic and Southern Oceans, Tellus B, 63, 823–830, 2011.

Rysgaard, S., Glud, R. N., Lennert, K., Cooper, M., Halden, N., Leakey, R. J. G., Hawthorne, F. C., and Barber, D.: Ikaite crystals in melting sea ice – implications for pCO_2 and pH levels in Arctic surface waters, The Cryosphere, 6, 901–908, doi:10.5194/tc-6-901-2012, 2012a.

Rysgaard, S., Mortensen, J., Juul-Pedersen, T., Sørensen, L. L., Lennert, K., Søgaard, D. H., Arendt, K. E., Blicher, M. E., Sejr, M. K., and Bendtsen, J.: High air–sea CO_2 uptake rates in nearshore and shelf areas of Southern Greenland: temporal and spatial variability, Mar. Chem., 128–129, 26–33, 2012b.

Rysgaard, S., Wang, F., Galley, R. J., Grimm, R., Lemes, M., Geilfus, N.-X., Chaulk, A., Hare, A. A., Crabeck, O., Else, B. G. T., Campbell, K., Papakyriakou, T., Sørensen, L. L., Sievers, J., and Notz, D.: Dynamic ikaite production and dissolution in sea ice – control by temperature, salinity and pCO_2 conditions, The Cryosphere Discuss., 7, 6075–6099, doi:10.5194/tcd-7-6075-2013, 2013a.

BGD
11, 7485–7519, 2014

Rysgaard, S., Søgaard, D. H., Cooper, M., Pućko, M., Lennert, K., Papakyriakou, T. N., Wang, F., Geilfus, N. X., Glud, R. N., Ehn, J., McGinnis, D. F., Attard, K., Sievers, J., Deming, J. W., and Barber, D.: Ikaite crystal distribution in winter sea ice and implications for CO_2 system dynamics, The Cryosphere, 7, 707–718, doi:10.5194/tc-7-707-2013, 2013b.

Semiletov, I. P., Makshtas, A., Akasofu, S. I., and Andreas, E. L.: Atmospheric CO_2 balance: the role of Arctic sea ice, Geophys. Res. Lett., 31, L05121, doi:10.1029/2003GL017996, 2004.

Søgaard, D. H., Thomas, D. N., Rysgaard, S., Norman, L., Kaartokallio, H., Juul-Pedersen, T., Glud, R. N., and Geilfus, N. X.: The relative contributions of biological and abiotic processes to the carbon dynamics in subarctic sea ice, Polar Biol., 36, 1761–1777, doi:10.1007/s00300-013-1396-3, 2013.

Takahashi, T., Sutherland, S. C., Wanninkhof, R., Sweeney, C., Feely, R. A., Chipman, D. W., Hales, B., Friederich, G., Chavez, F., Sabine, C., Watson, A., Bakker, D. C. E., Schuster, U., Metzl, N., Inoue, H. Y., Ishii, M., Midorikawa, T., Nojiri, Y., Kortzinger, A., Steinhoff, T., Hoppenma, M., Olafsson, J., Arnarson, T. S., Tilbrook, B., Johannessen, T., Olsen, A., Bellerby, R., Wong, C. S.„ Delille, Bates, N. R., and de Baar, H. J. W.: Climatological mean and decadal change in surface ocean pCO_2, and net sea–air CO_2 flux over the global oceans, Deep-Sea Res. Pt. II, 56, 554–577, 2009.

Taylor, P. D. and Feltham, D. L.: A model of melt pond evolution on sea ice, J. Geophys. Res.-Oceans, 109, C12007, doi:10.1029/2004JC002361, 2004.

Untersteiner, N.: Natural desalination and equilibrium salinity profile of perennial sea ice, J. Geophys. Res., 73, 1251–1257, 1968.

Weeks, W. F. (Ed.): On Sea Ice, Fairbanks, Alaska, 664 pp., 2010.

Zeebe, R. E. and Wolf-Gladrow, D.: CO_2 in Seawater: Equilibrium, Kinetics, Isotopes, Elsevier, 2001.

Zhou, J. Y., Delille, B., Eicken, H., Vancoppenolle, M., Brabant, F., Carnat, G., Geilfus, N. X., Papakyriakou, T., Heinesch, B., and Tison, J. L.: Physical and biogeochemical properties in landfast sea ice (Barrow, Alaska): insights on brine and gas dynamics across seasons, J. Geophys. Res.-Oceans, 118, 3172–3189, 2013.

BGD
11, 7485–7519, 2014

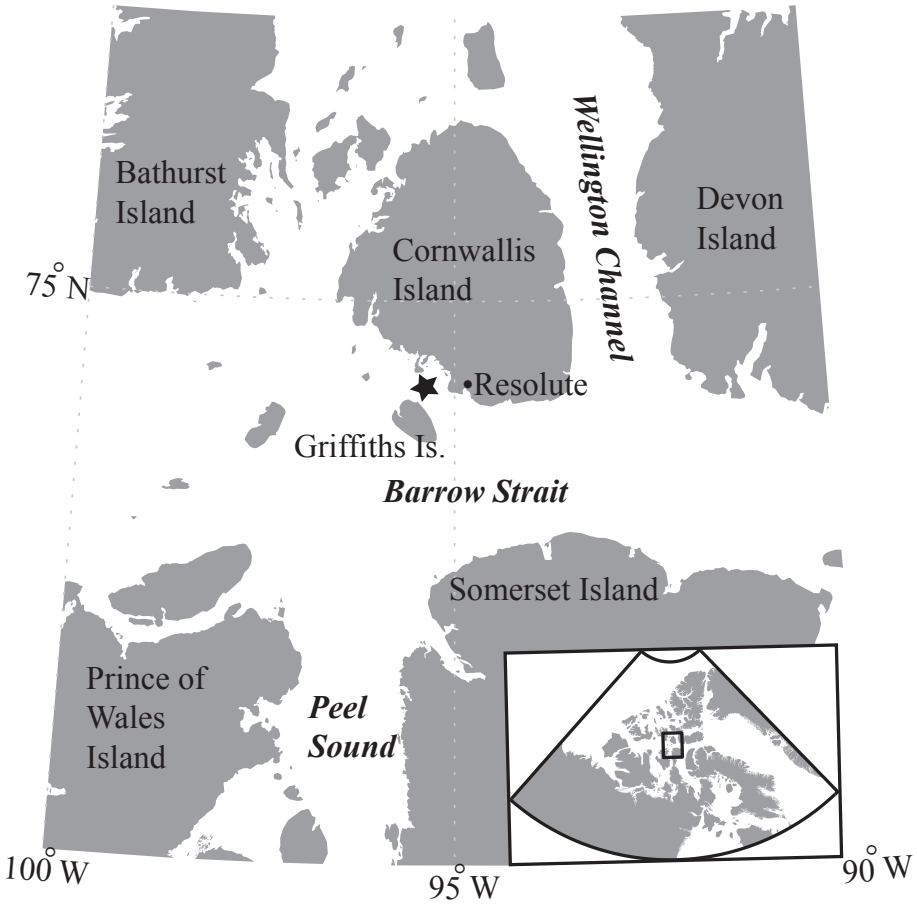

Figure 1. Location map of the sampling area in the Resolute Passage, Nunavut. The sampling site was located between Sheringham Point and Griffith Island (74.726° N, 95.576° W).

BGD
11, 7485–7519, 2014


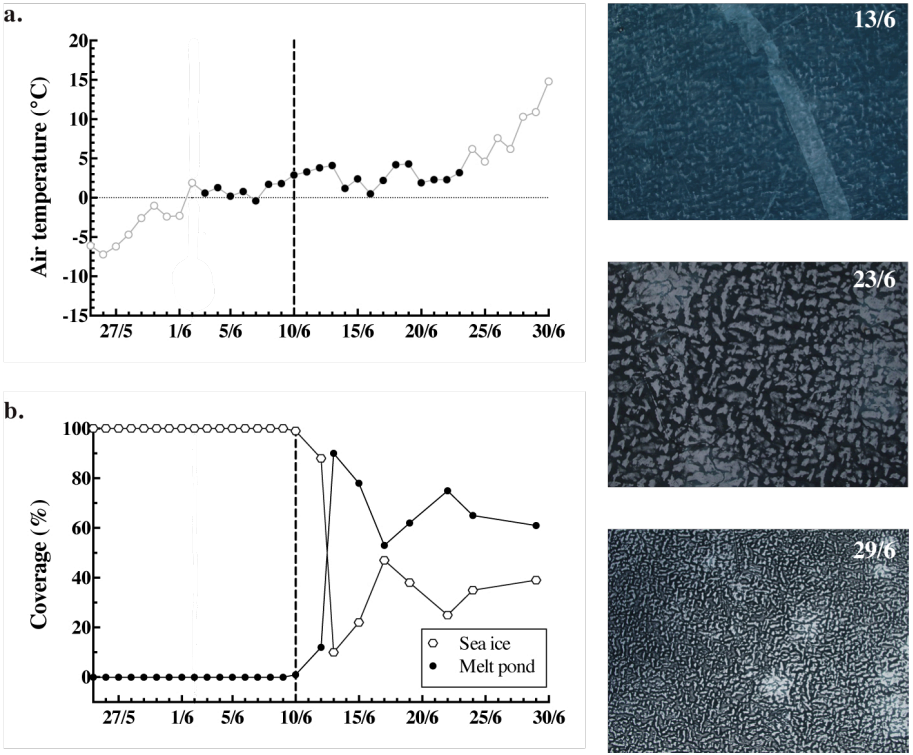

Figure 2. (a) Evolution of the atmospheric temperature in Resolute from the end of May to the end of June 2012. The black dots represent the air temperature during our survey (from 3 to 23 June). **(b)** Evolution of the melt ponds (black dots) and sea ice (white dots) fraction coverage at the sampling site. The bold dashed line on 10 June represents the initial formation of melt ponds at the surface of the ice cover. Aerial photo were taken over the field study site on 13 June (pond fraction = 0.9; width of the picture = 4472 m), 23 June (pond fraction = 0.65; width of the picture = 2212 m), 29 June (pond fraction = 0.61; width of the picture = 4426 m).

BGD
11, 7485–7519, 2014

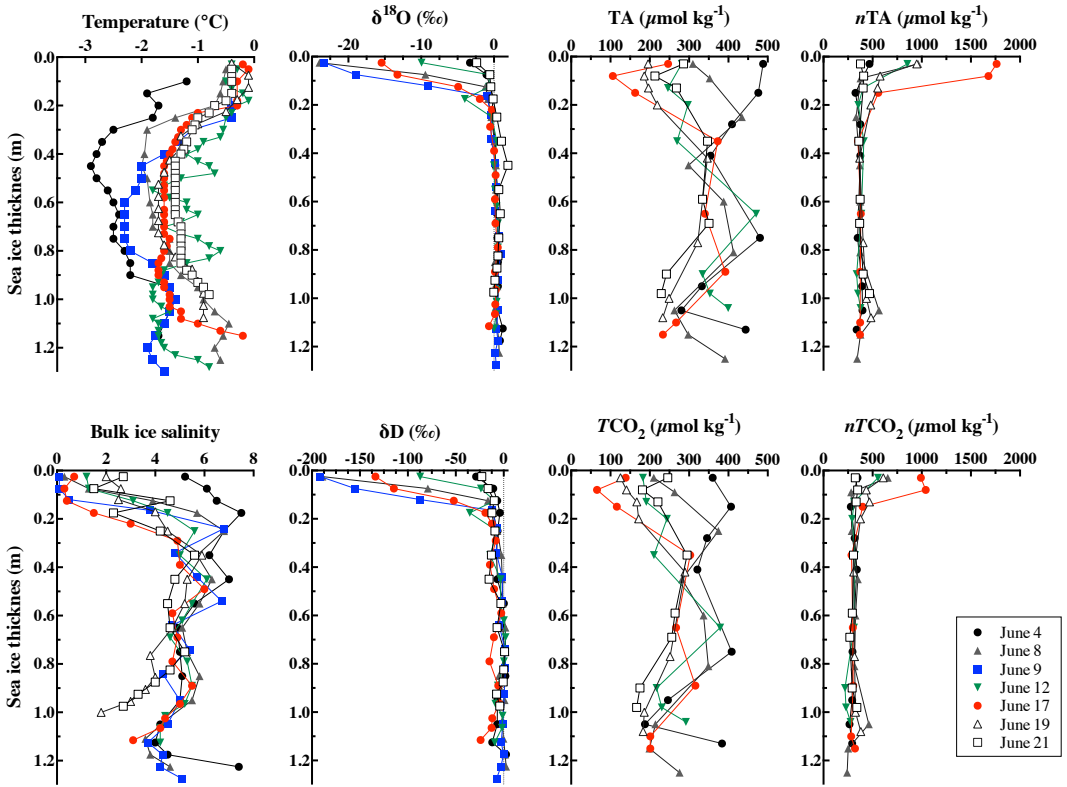

Figure 3. Sea ice profiles of temperature (°C), salinity, isotopic composition of $\delta^{18}O$ and δD (‰), TA_{ice} and nTA_{ice} (in μmol kg^{-1}), TCO_2 and $nTCO_{2\,ice}$ (in μmol kg^{-1}).

BGD
11, 7485–7519, 2014

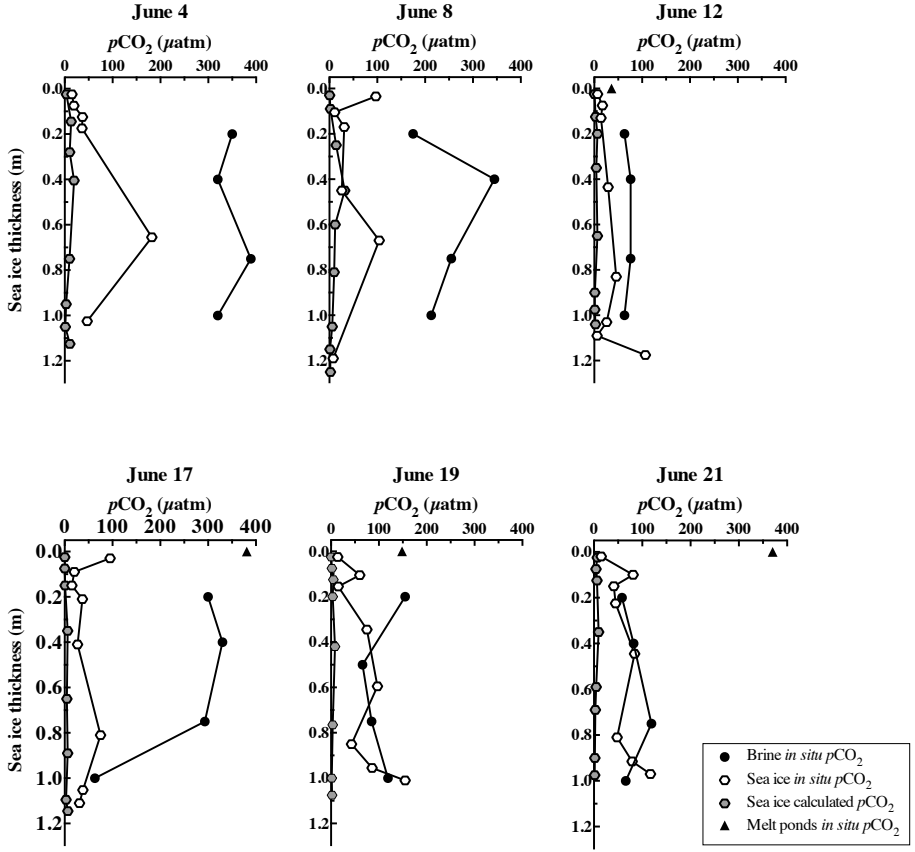

Figure 4. Sea ice profiles of pCO_2 (µatm) calculated from TA_{ice} and TCO_{2ice} (grey diamonds) and in situ bulk sea ice pCO_2 (white diamonds). The in situ brine and melt ponds pCO_2 are also represented (back dots and triangle, respectively).

BGD
11, 7485–7519, 2014

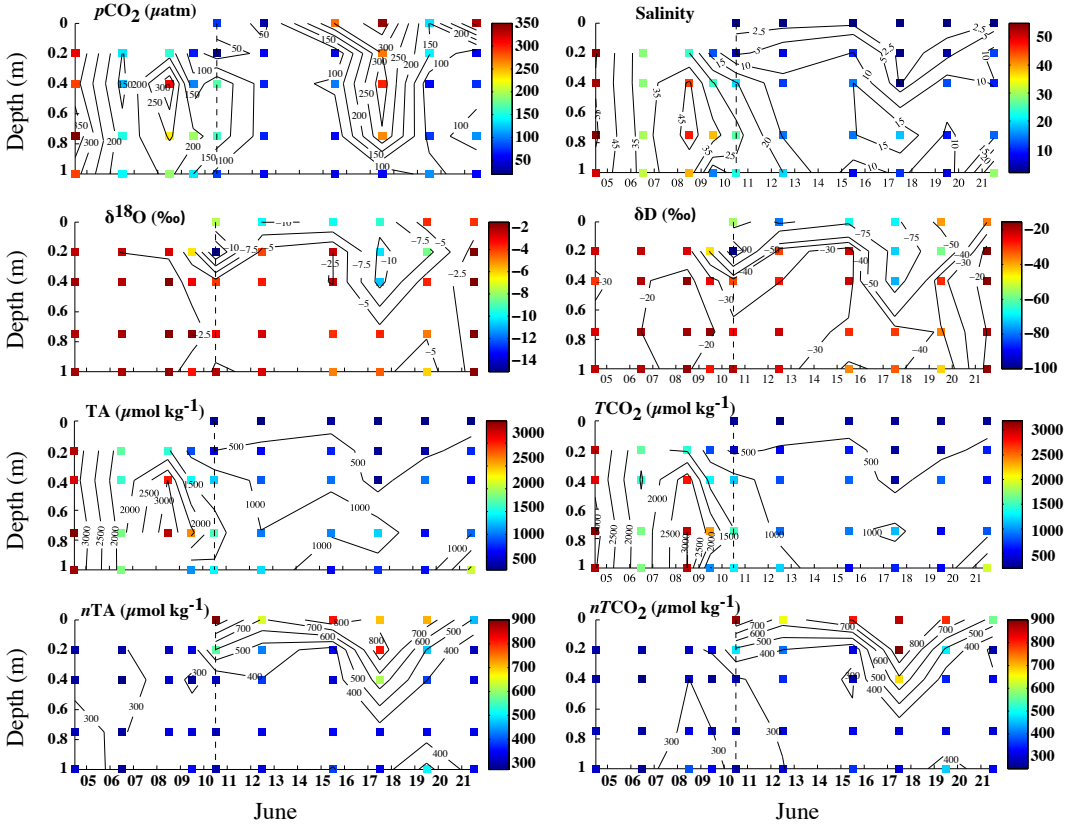

Figure 5. Profiles of in situ brine pCO_2 (in µatm), salinity, isotopic composition of $\delta^{18}O$ and δD (‰), TA_{br} and nTA_{br} (in µmol kg^{-1}), TCO_{2br} and $nTCO_{2br}$ (in µmol kg^{-1}).

BGD
11, 7485–7519, 2014

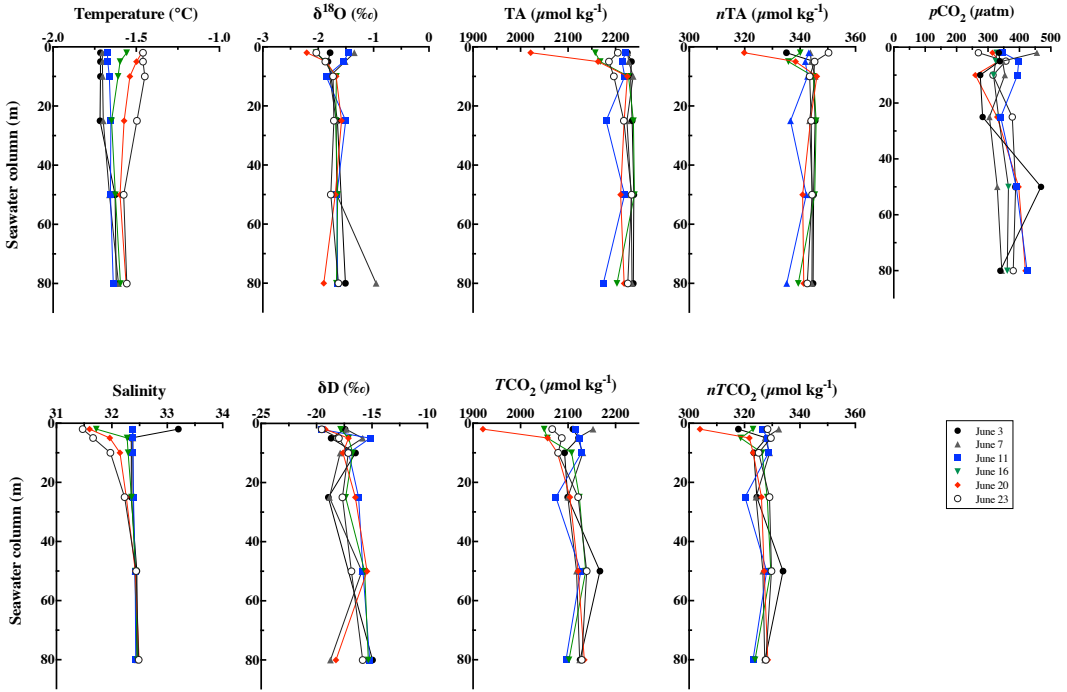

Figure 6. Water column profiles of temperature (°C), salinity, isotopic composition of $\delta^{18}O$ and δD (‰), TA and nTA (in µmol kg^{-1}), TCO_2 and $nTCO_2$ (in µmol kg^{-1}) and calculated pCO_2 (in µatm).

BGD
11, 7485–7519, 2014

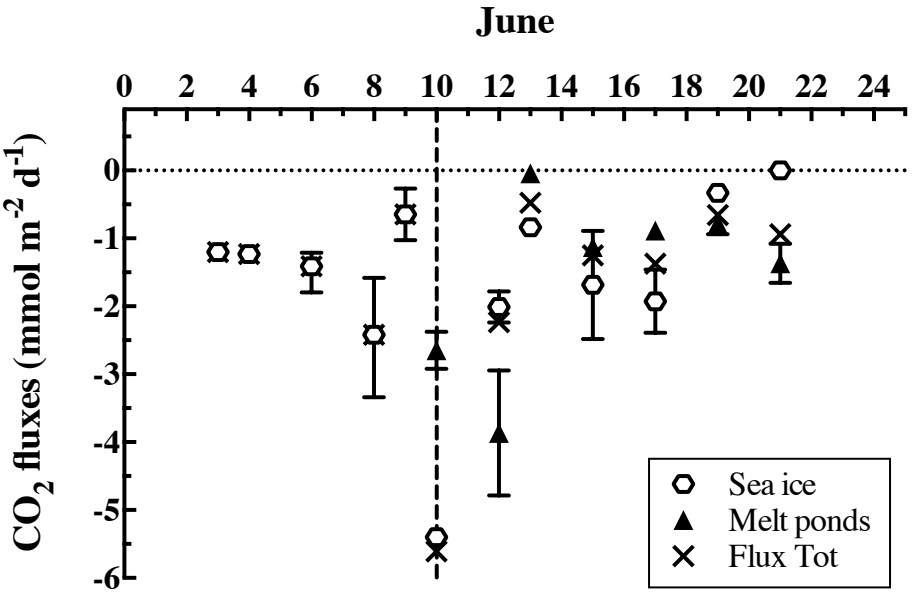

Figure 7. CO_2 fluxes (in mmol m^{-2} d^{-1}) measured over sea ice (white diamonds), melt ponds (black triangle). The total fluxes are represented by the black cross.

BGD
11, 7485–7519, 2014

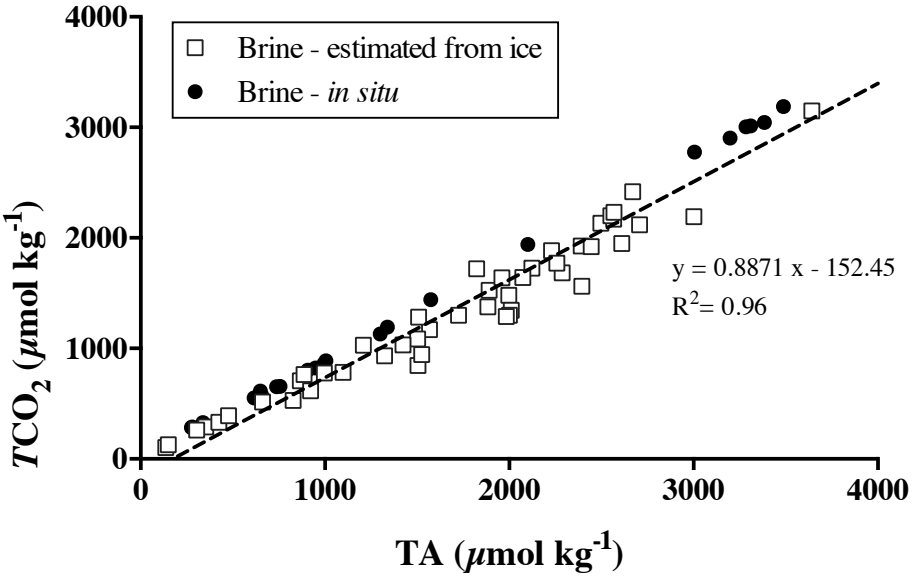

Figure 8. Relationships between TA and TCO_2 measured in the brine (black dots) and estimated from TA_{ice} and TCO_{2ice} (white dots).

BGD
11, 7485–7519, 2014

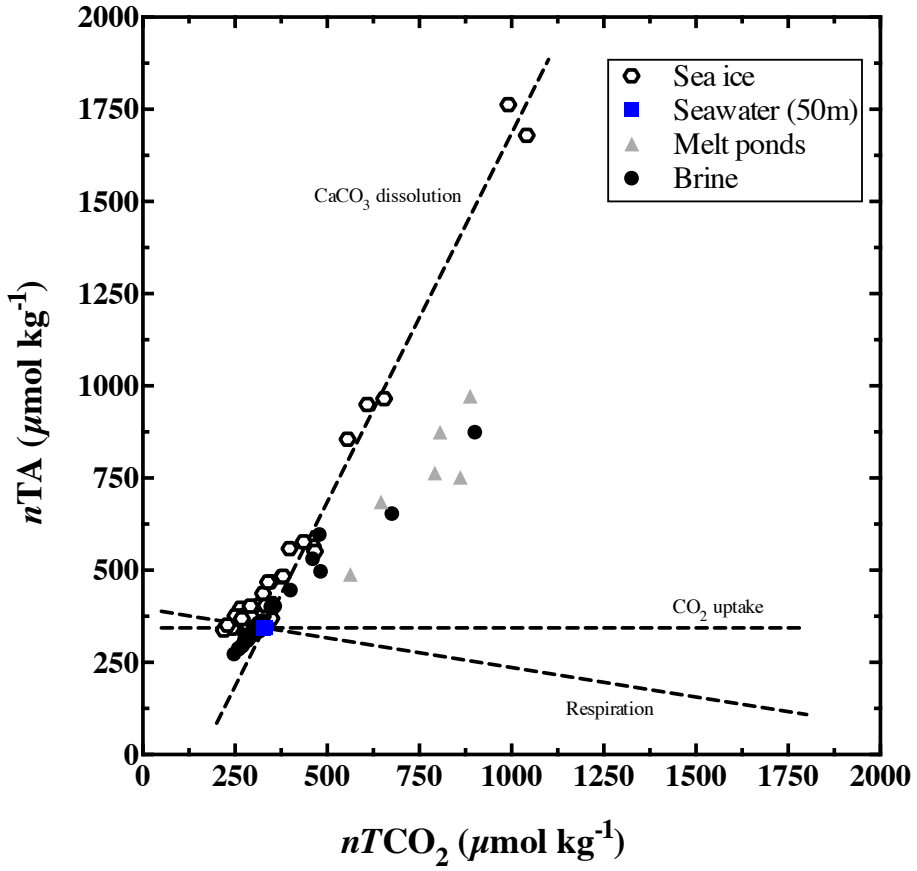

Figure 9. Relationship between the $nTCO_2$ and nTA (in μmol kg^{-1}) in bulk sea ice (white diamonds), melt ponds (grey triangle) and brine samples (black dots). The different dashed lines represent the theoretical evolution of nTA : $nTCO_2$ ratio following the precipitation/dissolution of calcium carbonate, release/uptake of $CO_{2(g)}$ and the impacts of the biology.

BGD
11, 7485–7519, 2014

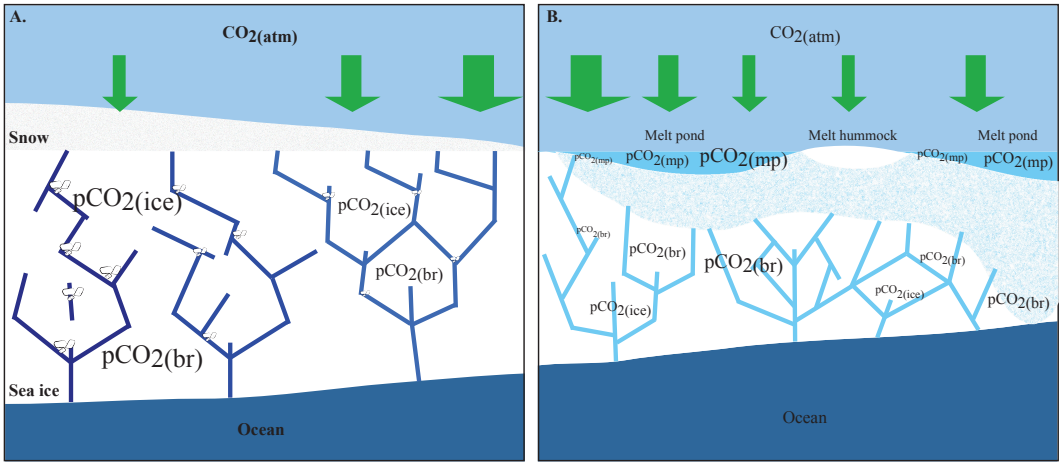

Figure 10. Illustration of the inorganic carbon dynamics of melt pond-covered first year sea ice. **(a)** The increase of the ice temperature and the decrease of the salinity, associated with the dissolution of ikaite crystals promote the decrease of the bulk ice and brine pCO_2. **(b)** Formation of melt ponds at the surface of the ice and percolation of meltwater into the ice matrix. The pCO_2 level is indicated by the size of the writing. The intensity of the CO_2 uptake is indicated by the size of the arrow.

BGD
11, 7485–7519, 2014